Development 139, 3442-3455 (2012) doi:10.1242/dev.081315

Principles of branch dynamics governing shape characteristics of cerebellar Purkinje cell dendrites

Kazuto Fujishima[1,2,‡], Ryota Horie[3,*], Atsushi Mochizuki[3] and Mineko Kengaku[1,2,4,‡]

SUMMARY

Neurons develop dendritic arbors in cell type-specific patterns. Using growing Purkinje cells in culture as a model, we performed a long-term time-lapse observation of dendrite branch dynamics to understand the rules that govern the characteristic space-filling dendrites. We found that dendrite architecture was sculpted by a combination of reproducible dynamic processes, including constant tip elongation, stochastic terminal branching, and retraction triggered by contacts between growing dendrites. Inhibition of protein kinase C/protein kinase D signaling prevented branch retraction and significantly altered the characteristic morphology of long proximal segments. A computer simulation of dendrite branch dynamics using simple parameters from experimental measurements reproduced the time-dependent changes in the dendrite configuration in live Purkinje cells. Furthermore, perturbation analysis to parameters in silico validated the important contribution of dendritic retraction in the formation of the characteristic morphology. We present an approach using live imaging and computer simulations to clarify the fundamental mechanisms of dendrite patterning in the developing brain.

KEY WORDS: Time-lapse imaging, Computer simulation, Purkinje cell, Mouse

INTRODUCTION

Dendrite morphologies of CNS neurons are highly diverse, depending on cell type and function (Gao, 2007). The architecture of dendritic arbors crucially affects the integration of inputs and propagation of signals, and, hence, determines the connectivity of neurons (London and Häusser, 2005; Branco and Häusser, 2010). The question of how neurons acquire their appropriate morphology is a major issue in the study of neuronal development (Whitford et al., 2002; Gao, 2007; Parrish et al., 2007; Jan and Jan, 2010).

Time-lapse visualization of growing dendrites in live preparations has shown that establishment of a dendritic tree is governed by a combination of local branch dynamics, including elongation, branching and retraction (Dailey and Smith, 1996; Portera-Cailliau et al., 2003; Wu and Cline, 2003; Emoto et al., 2004; Williams and Truman, 2004; Mumm et al., 2006). In spite of individual differences in branch patterns, the apparent homogeneity of dendrite shape of the same neuronal class suggests that there are cell type-specific rules for local branch dynamics, which might be affected by both genetic and environmental factors. Various molecular signals have been identified as regulators of dendritic arborization patterns (Jan and Jan, 2010). However, how the series of local branch dynamics build up cell class-specific dendrite shapes, and which specific steps of branch dynamics are regulated by each molecule, remain largely elusive.

Attempts have been made to reconstitute dendrite growth processes using mathematical models. Among these are growth models aimed at finding elementary rules of dendrite development that inform branch pattern variation. Stochastic growth models assume that dendritic growth is an outcome of serial stochastic processes (van Pelt and Uylings, 2002). Alternatively, mechanistic growth models reconstitute dendrite differentiation based on cellular mechanisms, including protein reaction dynamics (Luczak, 2006; Sugimura et al., 2007; Shimono et al., 2010). Most of these models employ hypothetical parameter sets, and thus lack a strong connection with actual dynamics in live cells.

The cerebellar Purkinje cell forms space-filling dendrites that extensively ramify non-overlapping branchlets in a single parasagittal plane (Ramon y Cajal, 1911). The non-overlapping dendrites of a Purkinje cell enable it to make hundreds of thousands of non-redundant synapses with parallel fibers (Napper and Harvey, 1988), which pass perpendicularly through the planes formed by Purkinje cell dendrites. Considerable efforts have been made to define anatomical characteristics of Purkinje cell dendrites (Berry et al., 1972; Berry and Bradley, 1976a; Mori and Matsushima, 2002; McKay and Turner, 2005) and underlying molecular mechanisms (Metzger and Kapfhammer, 2003; Kapfhammer, 2004; Shima et al., 2004; Ohkawa et al., 2007; Sotelo and Dusart, 2009; Tanaka, 2009; Li et al., 2010). Recent studies have focused on time-lapse observation of Purkinje dendrite arborization in vivo and in culture (Lordkipanidze and Dunaevsky, 2005; Tanaka et al., 2006; Tanabe et al., 2010). However, long-term observation over days to weeks of the gradual progression of Purkinje cell development has been challenging owing to the concurrent dynamic morphogenetic changes, including cell migration and deepening of the lobules in the cerebellum. It has also been difficult to distinguish specific dynamic parameters affected by genetic and

[1]Institute for Integrated Cell-Material Sciences (WPI-iCeMS), Kyoto University, Yoshida Honmachi, Kyoto 606-8501, Japan. [2]Laboratory for Neural Cell Polarity, RIKEN Brain Science Institute, Wako, Saitama 351-0198, Japan. [3]Theoretical Biology Laboratory, RIKEN Advanced Science Institute, Wako, Saitama 351-0198, Japan. [4]Graduate School of Biostudies, Kyoto University, Yoshida Honmachi, Kyoto 606-8501, Japan.

*Present address: Department of Communications Engineering, College of Engineering, Shibaura Institute of Technology, Tokyo 135-8548, Japan
‡Authors for correspondence (fujishima@icems.kyoto-u.ac.jp; kengaku@icems.kyoto-u.ac.jp;)

Accepted 27 June 2012

pharmacological manipulations deforming dendrites. The mechanisms and rules of dendrite formation in the Purkinje cell are, thus, still largely unknown.

In this study, we conducted long-term time-lapse observation of dendrite formation of Purkinje cells in culture, for up to several days with short time intervals. Using quantitative analyses and computer-aided simulation, we identified the fundamental rules of growth dynamics that govern the construction of the characteristic dendrite patterns in Purkinje cells.

MATERIALS AND METHODS

Mice

Mice were handled in accordance with the Animal Experiment Committee of the RIKEN Brain Science Institute and Kyoto University.

DNA constructs, adeno-associated virus (AAV) injection and immunohistochemistry

The PKD1 K618N mutant was created by the QuickChange Site-Directed Mutagenesis Kit (Agilent), which was fused with mCherry-tag and cloned into pAAV-CAG vector. AAV-CAG-EGFP and AAV-CAG-TdTomato (adeno-associated virus vector carrying EGFP/TdTomato under the CMV enhancer and chicken β-actin promoter) were constructed and injected as previously described (Kaneko et al., 2011). Detailed methods for immunostaining and confocal analyses of labeled Purkinje cells were described previously (Kaneko et al., 2011). Antibodies used for immunostaining were as follows: mouse anti-calbindin D28K (Swant); rabbit anti-Pax6 (Covance); rabbit anti-DsRed (Clontech); chick anti-GFP (Invitrogen); rabbit anti-PKD1 (SantaCruz); rabbit anti-PKD2 (Calbiochem); rabbit anti-PKD3 (Calbiochem); rat anti-Thy1 (CD90.2, BioLegend); Alexa488- or Alexa568-conjugated anti-rabbit, anti-mouse or anti-chick IgG (Invitrogen).

Time-lapse imaging and morphological analysis of Purkinje cells in primary cultures

Purkinje cells from postnatal day (P) 0 mouse cerebella were dissociated and plated on a glass-based dish coated with poly-D-lysine in DMEM/F12 supplemented by 10% FBS. Two hours after plating, media were replaced by maintenance medium containing DMEM/F12, 0.1 mg/ml bovine serum albumin, 2.1 mg/ml glucose, 3.9 mM glutamine, a modified N3 supplement (8 μM progesterone, 20 μg/ml insulin, 100 μM putresine, 30 nM selenium dioxide) and 1% penicillin-streptomycin. Plasmids containing PKD1-K618N and TdTomato were transfected by nucleofection of dissociated cells from one and a half cerebella using 10 μg of each plasmid with nucleofector protocol O-03 (Wagner et al., 2011). Transfected cells were observed using a confocal microscope (FV1000, Olympus) with 40× air UPlan SApo objective. For time-lapse imaging, Purkinje cells were GFP-labeled by adding 1 μl of AAV-CAG-EGFP [10^9-10^{10} plaque-forming units (pfu)/ml] to the medium. Labeled cells were observed every 3 hours with an incubation microscope (LCV100, Olympus) using a 20× objective (numerical aperture 0.7, Olympus). Dendrites were traced and reconstructed with the aid of Neurolucida software (MBF Bioscience) for quantitative analysis using Neurolucida Explore and ImageJ (NIH). Branch angle was defined as the angle between the lines produced by a branch point and the branch points or dendritic tips terminating each of the daughter segments. All data are expressed as mean ± s.e.m. unless otherwise indicated. Comparisons of variables between two groups were made by Student's *t*-test. A probability value of $P<0.05$ was considered to be significant.

Time-lapse imaging of organotypic slice culture of the cerebellum

Mice were injected in the cerebellum with AAV-CAG-TdTomato at P0. Cerebella were dissected and embedded in 3.5% agarose at P7. Vibratome sections (370 μm) were plated on a Millicell-CM plate (Millipore), settled in a culture medium at 37°C in a CO_2 incubator for 2-5 hours, and then observed with a confocal microscope (FV1000, Olympus) with 20× air UPlan SApo objective (numerical aperture=0.75) at 8-hour intervals.

Pharmacological manipulation

Pharmacological agents used for primary dissociation culture and organotypic culture were as follows: Gö6976 (Calbiochem), Gö6983 (Calbiochem), CGP41251 (Alexis Biochemicals), LY333531 (Alexis Biochemicals), Ro-31-8220 (Calbiochem), CID755673 (Sigma-Aldrich), phorbol-12-myristate-13-acetate (phorbol ester, Calbiochem). These agents were bath-applied one or two hours before recording.

Reconstruction of dendrite dynamics in a computer-aided simulation

Numerical simulations and quantitative analysis were carried out in Matlab (Mathworks).

Framework of the model

Dendrite growth dynamics was modeled on two-dimensional space following previous mathematical models (van Pelt et al., 2003) as repeats of operations of unit fragments at the terminals of dendrites. The 'elongation' and 'branching' were alternative processes that occurred at each terminal every 3 hours, and were represented by the addition of one and two unit fragment(s), respectively (supplementary material Fig. S3). After the 'elongation' or 'branching', one choice of operations in the 'contact treatment' was carried out depending on the condition number.

The algorithm

The algorithm carried out the following sequence: (1) One of the growing terminals is selected. (N.B. All terminals are growing terminals at the initial time point); (2) 'Elongation' or 'branching' process is selected and carried out (determined by the branching probability); (3) The new fragments are tested to determine whether they are contacted by other branches. Each of the contacted terminals is processed for a 'contact treatment'; (4) Steps 1-3 are repeated until the calculation time (step number)*(terminal number)*Δt reaches the given maximum time.

Initial state

The soma was approximated by a circle with a radius of 8.65 μm, which was determined from somal area measured in real cultured Purkinje cells using the equation $r=\sqrt{(\text{area}/\pi)}$ (somal area; 236±6.1 μm^2, n=16). Primary dendrites were initiated at 0 hour with a single unit without a branch. The position and the direction of the primary dendrites were determined by distributions of two classes of angles: the 'divergence angle of primary dendrites' and the 'direction angle of primary dendrites' (supplementary material Fig. S3A).

Elongation process

A unit fragment is added at each terminal of a dendrite with the elongation probability $p_e=r_e\Delta t=0.74$, where the Δt is 3 hours, corresponding to the observation interval in experiments. The 'deviation angle', the angle between mother fragment and newly added daughter fragment, is assumed to follow a homogeneous distribution from –5° to +5°.

Branching process

Two unit segments are added at each terminal with the branching probability $1-p_e=1-r_e\Delta t=0.26$. Directions of two daughter segments are determined by distributions of two angles: the 'divergence angle of branching' and the 'direction angle of branching' (supplementary material Fig. S3C). The distribution of the divergence angle was approximated by a log-normal distribution with an average value of 65°, whereas that of the direction angle was assumed to be a normal distribution with average 3.39°. Values were determined from measurement of real cells as shown in Fig. 3.

Contact treatment

If a new added fragment contacts other branches, either of the following operations is carried out:

Condition 1 (contact-dependent retraction): the branch including the added fragment is stopped from growing and then eliminated 7 steps later. The entire dendritic segment is removed from the branching root (supplementary material Fig. S3D).

Condition 3 (contact-dependent stalling): the terminal of the branch with the added fragment becomes a 'non-growing' terminal, which will never be selected as a growing terminal (supplementary material Fig. S3D).

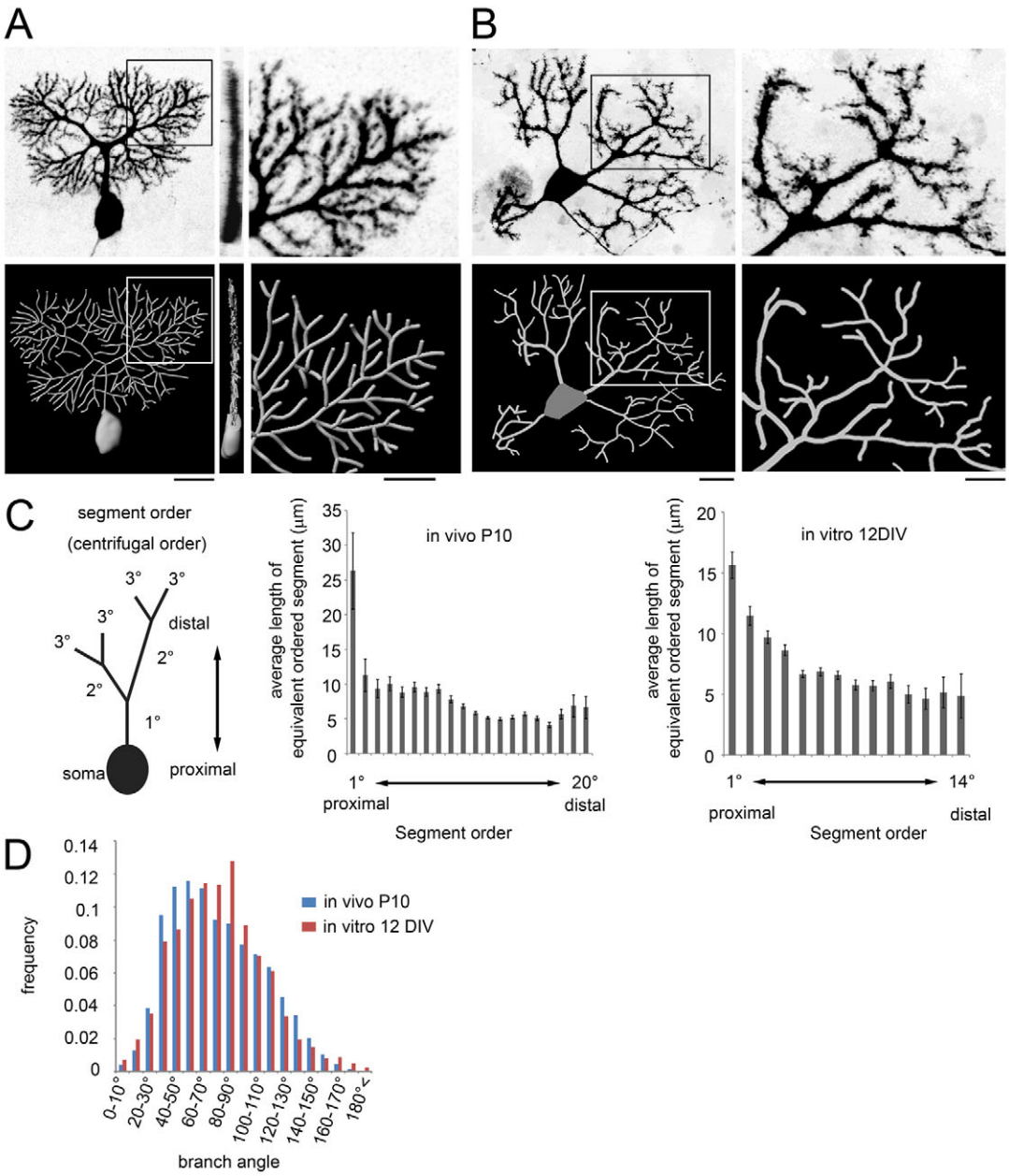

Fig. 1. Morphological characteristics of Purkinje cells in vivo and in dissociation culture. (**A**) Confocal (upper) and graphic (lower) images of a GFP-labeled Purkinje cell in vivo at P10. Sagittal (left) and coronal (middle) views are shown. Boxed regions are magnified on the right. (**B**) Representative images of a Purkinje cell in dissociation culture at 12 DIV stained with anti-calbindin (upper). Graphical images were constructed by Neurolucida (lower). Boxed regions are magnified on the right. (**C**) The mean length of equivalent ordered segments in vivo (middle, P10; *n*=21) and in dissociation culture (right, 12 DIV; *n*=20). The dendritic segments are numbered in a centrifugal order (diagram on left). Error bars represent s.e.m. (**D**) The distributions of branch angles in vivo and in dissociation culture (blue, P10 in vivo, 75.7° ± 13.5, *n*=2022 from 21 cells; red, 12 DIV in culture, 76.3° ± 33.3, *n*=1392 from 20 cells; mean ± s.d.). Scale bars: 20 μm in left panels in A,B and middle panel in A; 10 μm in right panels in A,B.

Condition 2: either of 'retraction' or 'stalling' processes is selected with the probability shown in Fig. 4D. The probability is approximated by a quadratic $0.058T^2 - 0.0072T + 0.0054$, where T is calculation step ($1 \leq T \leq 31$).

RESULTS

High complexity of Purkinje cell dendrite arborization both in vivo and in vitro

Purkinje cell soma extend multiple dendrites in random orientations during the first postnatal week in mice. A single or a few primary dendrites are determined during the second postnatal week, which extend and branch in a single parasagittal plane until the sixth week (McKay and Turner, 2005; Sotelo and Dusart, 2009). Figure 1A shows a typical Purkinje cell in the 10-day-old (P10) mouse labeled with enhanced green fluorescent protein (EGFP) by AAV-mediated gene transfer (Hirai, 2008; Kaneko et al., 2011). We monitored dendrite morphometry using three-dimensional confocal reconstruction of labeled cells. Consistent with previous studies (Berry and Bradley, 1976b; Berry and Flinn, 1984), the segment length between two branching nodes was longer for proximal

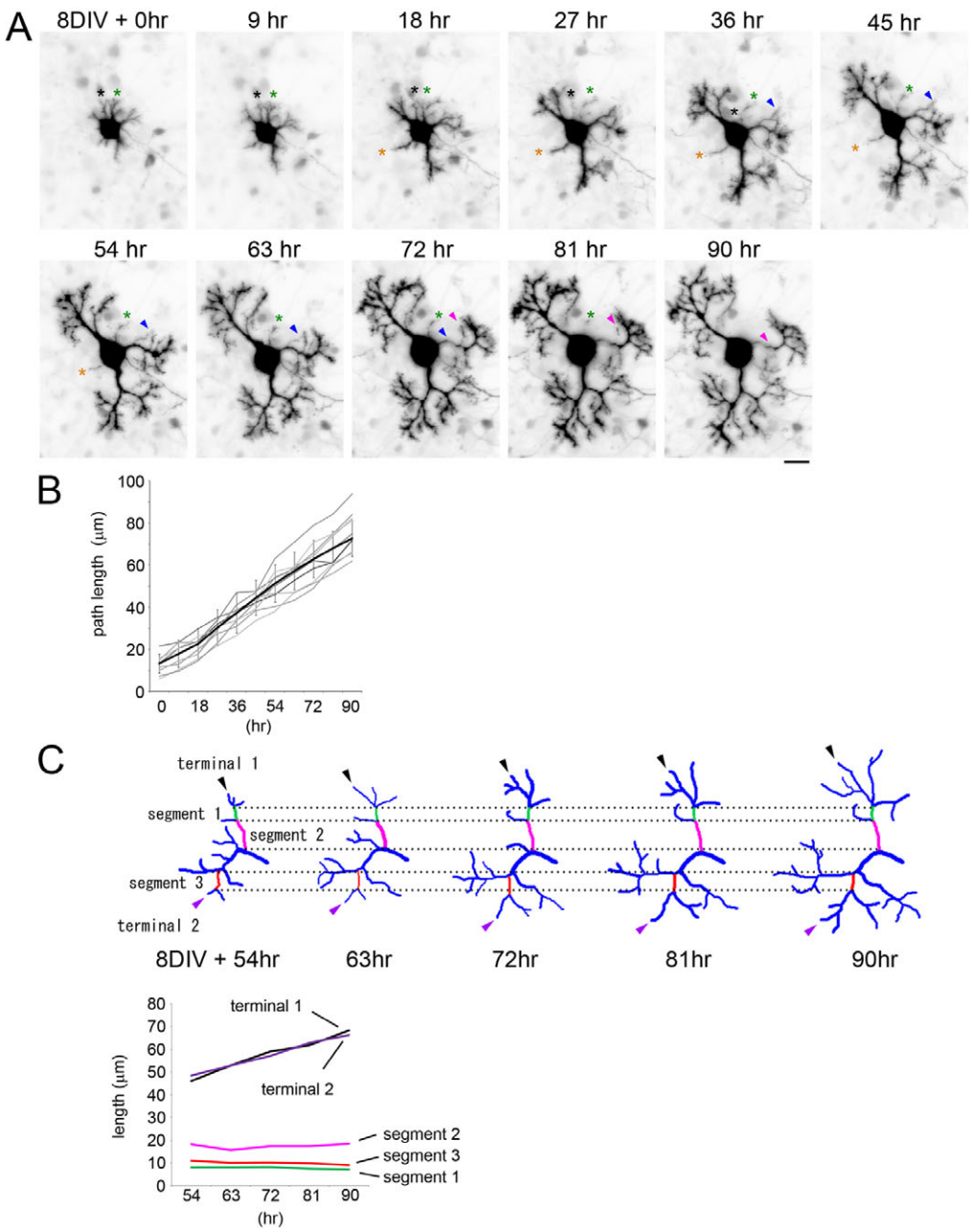

Fig. 2. Purkinje cell dendrites constantly grow at distal tips. (**A**) Time-lapse images of developing Purkinje cell dendrites in culture. Images were obtained at 3-hour intervals for up to 90 hours. Representative images (9-hour intervals) are shown. Some primary dendrites (asterisks) and growing branches (arrowheads) were retracted during observation. Scale bar: 20 μm. (**B**) Time-dependent change in the path length of dendrites. The foremost growing terminal of each primary dendrite was assessed for the path length from the soma to terminal. Data from ten individual terminals (gray lines) and the average value of 33 terminals (black line) are shown (mean ± s.d.). (**C**) Time-dependent changes in the path length of terminals and internal segments. Displacement of terminal tips and nodes of internal segments were traced as shown in the upper diagrams. Growing dendritic arbors with no branch retractions during observation were selected (see Fig. 4).

segments, whereas it decreased and plateaued in distal segments at about 5.72±0.099 μm (n=1771 segments of 10th order and above from 21 cells; Fig. 1C, left and middle).

The morphometric characteristics of Purkinje cell dendrites can be partly reconstructed in a dissociation culture (Fig. 1B)(Calvet et al., 1985; Hirai and Launey, 2000; Tanaka et al., 2006; Kawaguchi et al., 2010). Overall arboreal size and complexity was smaller in the dissociation culture that is deficient in trophic and structural support from neighboring cells within the tissue. However, the spatial distribution of dendrites showed striking parallels with those in vivo; dendrites formed non-overlapping arbors with longer proximal segments and constant distal segments of 5.41± 0.37 μm (n=112 segments of 10th order and above from 20 cells; Fig. 1C, right). The frequency distributions of branch angles were also comparable in vivo and in vitro (Fig. 1D). Thus, the mechanisms of branch formation in Purkinje cells are at least partly conserved in culture.

Time-lapse observation of dendritic outgrowth

We next performed long-term time-lapse observation of the dynamics of dendrite outgrowth in Purkinje cells in dissociation cultures. Purkinje cells were visualized by infecting with AAV-CAG-EGFP at 0 days in vitro (DIV) (Niwa et al., 1991; Kaneko et al., 2011). Infection with AAV induced little or no morphological changes in Purkinje cells (Hirai, 2008) (supplementary material Fig. S1A). Multiple thick dendrites emerged and initiated extension at ~8 DIV, concomitant with the timing of initiation of dendrite outgrowth in vivo. We monitored dendrite outgrowth of Purkinje cells from 8 to 12 DIV (Fig. 2A; supplementary material Movie 1). About six to ten stem dendrites were initiated around the soma at 8 DIV, half of which were degraded within 48 hours (Fig. 2A, asterisks; see also Fig. 6I). Persistent dendrites grew radially from the soma by repeated elongation and branching. The growth of dendrites appeared to be rather constant without drastic changes in overall

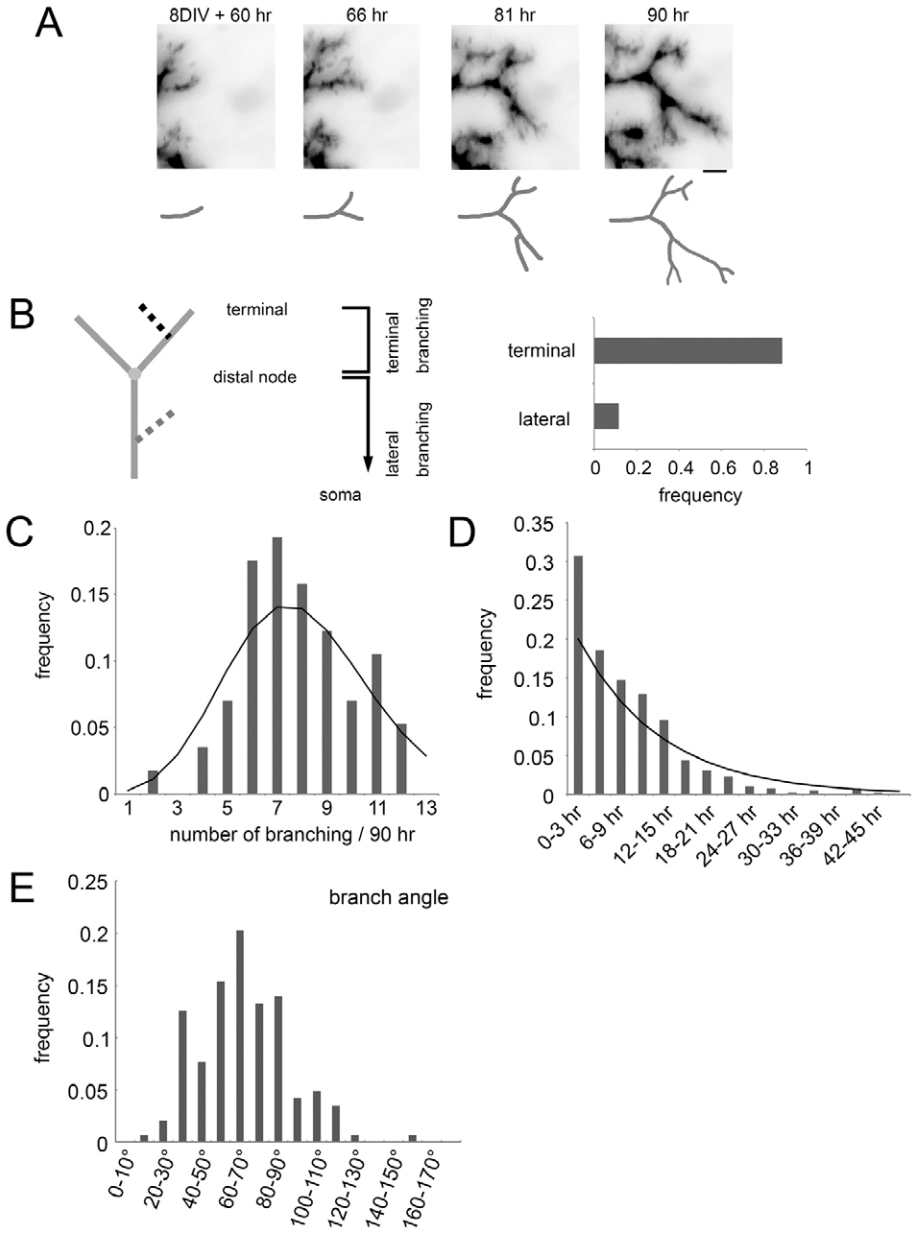

Fig. 3. Purkinje cell dendrites branch stochastically at distal tips. (**A**) Representative time-lapse images of branching dendrites. Optical traces are shown below. Repetitive dichotomous branching was observed at the terminals. Scale bar: 5 μm. (**B**) The branching patterns in Purkinje cells. Left: schematic diagram of branch type. New branch formation in the distal-most segment is defined as terminal branching (black dotted line), whereas that in any internal segments located proximally to the distal-most node (gray dotted line) is defined as lateral branching. Right: the frequency of terminal and lateral branching in time-lapse images (*n*=457 newly formed branches from 19 cells). (**C**) Histogram distribution of the number of branching events experienced by a growing terminal over a 90-hour period (*n*=57). Solid line represents Poisson distribution. (**D**) The frequency distribution of time intervals between two serial branching events. The solid line represents an exponential curve based on a Poisson process. (**E**) The distribution of angles made by newly formed sister branches (*n*=457 branching events from 19 cells).

arrangement. Retraction of growing branches was also observed (Fig. 2A, arrowheads). Thus, the basic three dynamics seen in other cell classes – elongation, branching and retraction – were observed in Purkinje cells. We next conducted quantitative evaluation of each dynamic.

Purkinje cell dendrites elongate constantly at the tips

First, we focused on the elongation process. We monitored the growing speed by tracing the displacement of individual dendritic tips in image sequences from 8 DIV to 12 DIV (Fig. 2B). Dendritic tips displaced distally from the soma at constant speeds with relatively small individual variations at an average of 0.66±0.02 μm/hour (*n*=33 dendrites from 11 cells). To investigate whether dendrites elongated at the tip (terminal elongation) or by each segment throughout the entire dendrite (segment elongation), image sequences were compared to measure time-dependent changes in the segment length and translocation of distal tips. As depicted in Fig. 2C, the distal-most region extended linearly, whereas proximal segments were rather static. These results indicate that Purkinje dendrites elongate at a constant speed by terminal elongation.

Branching occurs by stochastic terminal bifurcation at variable angles

Branches can be formed either by extension of collaterals from the dendritic shafts (lateral branching) or by division of growing tips (terminal branching) (Berry and Flinn, 1984; Sugimura et al., 2003). Time-lapse images revealed that most of the branching processes in Purkinje cells took place at or near the growing terminals (Fig. 3A; supplementary material Movie 2); nearly 90% of branching events occurred within the distal-most segments (Fig. 3B). The other 10% were lateral branching, but most of these events took place at distal regions near the terminal segment of the dendrite. By contrast, sprouting of collaterals in the proximal dendritic shafts was scarcely observed. Together with the results described above, Purkinje dendrites predominantly undergo

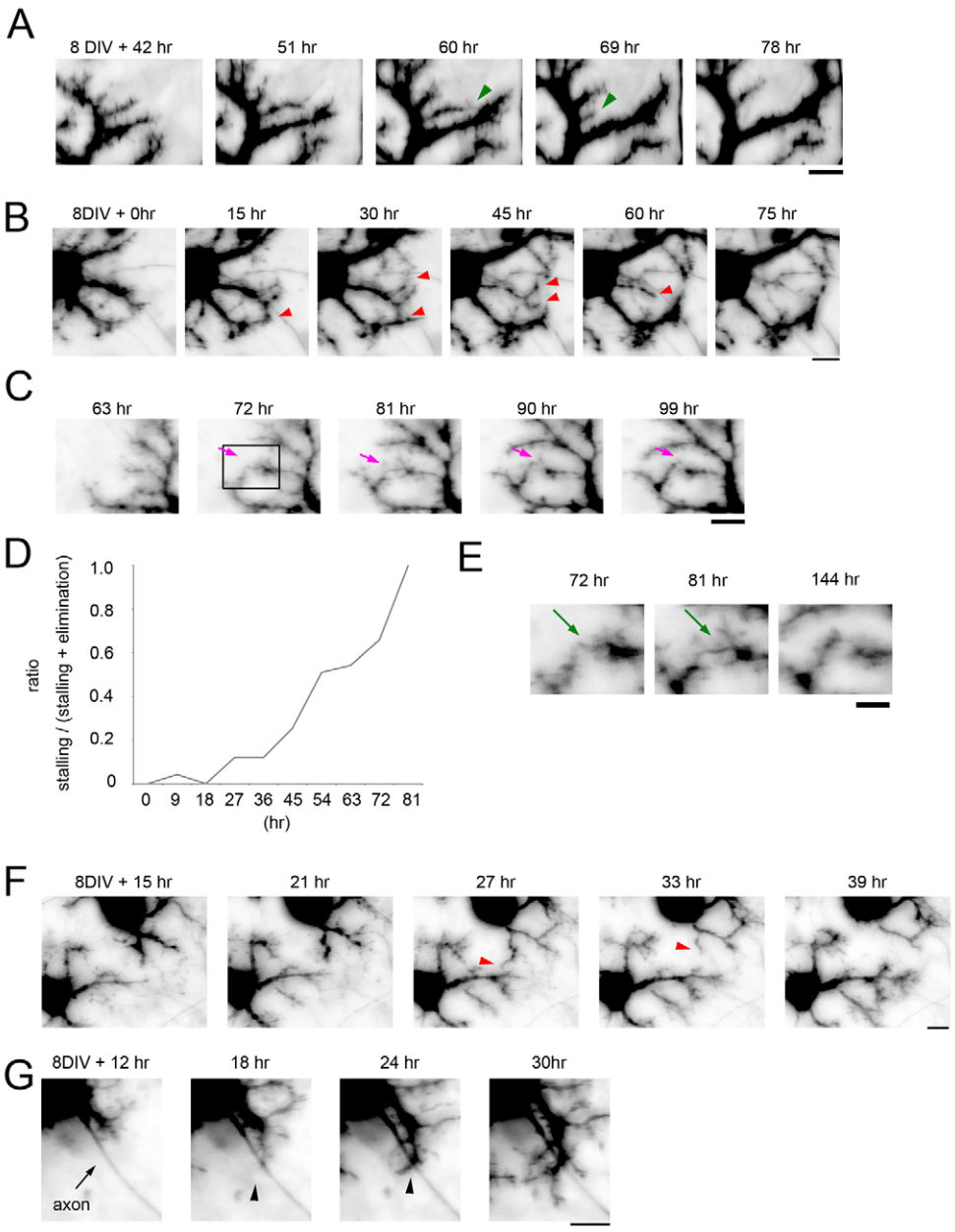

Fig. 4. Growing dendrites are retracted or stalled by contacts with other dendrites. (**A**) Representative sequential images of retracting dendrites. Terminal tips contacted with other dendrites (arrowhead) were retracted to the proximal node and resorbed within 18 hours. (**B**) Dendritic contacts (arrowheads) at earlier stages induced elimination at higher incidence. (**C**) Dendritic contacts at later stages induced stalling rather than retraction. Dendrites (arrows) stopped growing and stabilized after the contact. (**D**) Time-dependent changes in contact-induced repulsion. The ratio of stalled dendrites to retracted dendrites is plotted as a function of the time of dendritic contacts. (**E**) Enlarged views of dendritic tips in contact (boxed region in C). Filopodial protrusions that interacted with neighboring dendritic tips (arrows) disappeared after the branch was stabilized (144 hours). (**F**) Contacts between dendrites from neighboring cells (arrowheads) induced branch retraction. (**G**) Contact with the axon (arrow) never induced retraction or stalling of the dendrite (arrowheads). Scale bars: 10 μm.

elongation and branching at active zones in the growing terminals. Branching of growing terminals occurred stochastically, so that the frequency distribution of branching events was approximated by a Poisson distribution for 90 hours (Fig. 3C; average frequency 0.087±0.003 times/hour; n=57 dendritic terminals from 19 cells). Inter-branch intervals with respect to time distributed exponentially as predicted from a Poisson process (Fig. 3D). Angles formed between emerged sister branches were distributed with a mean ± s.d. of 65±21.2° (n=143 branches from four cells in time-lapse movies; Fig. 3E).

Dendritic retraction is induced by dendro-dendritic contact

Serial images indicated retraction (elimination) of branches, which was triggered by contacts (or tight apposition) between growing dendrites. Dendritic tips immediately stopped growing after encountering a neighboring dendrite or the soma, and were then retracted to the proximal branching node by one or two segments in ~20 hours (Fig. 4A; supplementary material Movie 3). By contrast, the dendritic shafts that were hit by growing tips from the side largely remained intact. Contacts between growing tips induced retraction of either (84%) or both (16%) tips to the proximal node(s) (Fig. 4B). The contact-dependent dendritic retraction was more evident in earlier stages of observation (from 8 DIV) and, thus, many of the initial stem dendrites were eliminated by dendro-dendritic contacts. Some of the initial stem dendrites were eliminated without experiencing obvious contact with other dendrites (e.g. yellow asterisks in Fig. 2A). Growing dendrites were gradually stabilized, so that dendro-dendritic contacts induced stalling of the terminals but not the subsequent branch retraction in later stages (Fig. 4C). The ratio of ‘stalled’ terminals among contacted dendrites increased non-linearly and reached close to 100% at the end of observation at 12 DIV (Fig. 4D). Interaction between dendrite branches was often mediated by

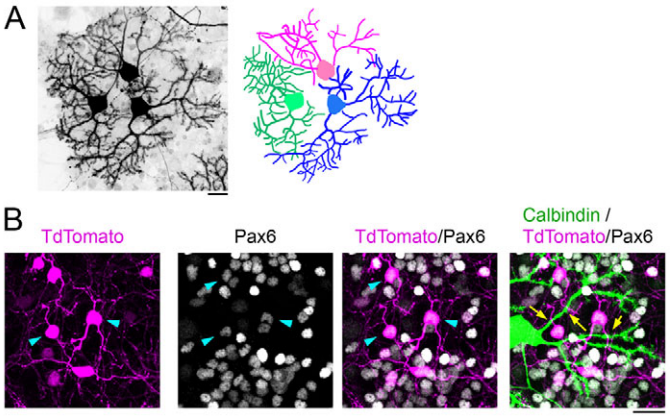

Fig. 5. Dendritic tiling of cultured Purkinje cells. (**A**) Left: Purkinje cells juxtaposed to other Purkinje cells in culture avoid dendritic overlaps. Right: graphic image of dendrite arbors. (**B**) Dendrites of a Purkinje cell (calbindin, green) and granule cells (magenta) crossed with each other in the dissociation culture at 11 DIV. The shape of Pax6-positive granule cells (white) were visualized by transfecting TdTomato. Arrowheads point to cell bodies of the labeled granule cells. Arrows indicate dendrite crossings between the Purkinje cell and granule cells. Scale bars: 20 μm.

filopodia-like motile protrusions. These protrusions disappeared in the stalled dendrites after contact, so that the tips of dendrites were dissociated from each other and stabilized in a non-overlapping arrangement (Fig. 4E).

Contact-dependent dendritic repulsion (retraction and stalling) seen in the present study, has been implicated in the self-avoidance mechanism that ensures a space-filling dendrites in invertebrate sensory neurons (Gan and Macagno, 1995; Grueber et al., 2003; Emoto et al., 2006; Han et al., 2012; Kim et al., 2012). Homotypic repulsive interactions have been shown to act not only between branches of the same cell but also between neighboring cells of the same type. Similarly, dendro-dendritic contacts between neighboring Purkinje cells induced retraction and stalling of branches (Fig. 4F, Fig. 5A). By contrast, dendrites of granule cells frequently overlapped with Purkinje cell dendrites in culture (Fig. 5B). In addition, contacts with the axon did not change the behavior of growing dendrites, indicating that contact-dependent repulsion is specific for homotypic dendro-dendritic interactions in Purkinje cells (Fig. 4G).

The effect of PKC inhibition on the dynamics of dendrite formation

We next searched for conditions that specifically altered certain parameters of dendrite dynamics. Previous studies have implicated protein kinase C (PKC) as a regulator of dendritic outgrowth in Purkinje cells (Metzger and Kapfhammer, 2003; Kapfhammer, 2004): pharmacological inhibition of PKC induces excess branch formation, which led to the assumption that PKC signaling negatively regulates branching. We first confirmed that Purkinje cells grown in the presence of a PKC inhibitor Gö6976 exhibited complicated dendritic arbors with higher spatial density (Fig. 6A). Next, time-lapse observation was performed in the presence of Gö6976 (Fig. 6B; supplementary material Movie 4). Dendritic terminals were constantly extended at a slightly but significantly lower speed in Gö6976-treated cells (Fig. 6C; control: 0.66±0.02 μm/hour, n=33; Gö6976: 0.47±0.02 μm/hour, n=36; P<0.01). Unexpectedly, the branching frequency was significantly lower in Gö6976-treated cells compared with untreated control cells, despite the crowded appearance of dendrites (Fig. 6D; control: 0.087±0.003 times/hour, n=57 dendritic terminals; Gö6976: 0.054±0.003 times/hour, n=40; P<0.01). As a result, the branching probability per unit length of dendrites was almost comparable in control and Gö6976-treated cells (control: 0.137±0.004; Gö6976: 0.119±0.008; P>0.05). What causes the crowded appearance of Gö6976-treated cells? A notable feature of Gö6976 treatment was a drastic suppression of branch retraction after dendro-dendritic contacts (Fig. 6E,F; supplementary material Movie 5). In most cases, branches stalled after collision with other branches, but never retracted or crossed over the contacted branches thereafter.

Next, we investigated how changes in dynamics induced by Gö6976 affected the entire structure of dendrites. There were no significant changes in the total dendritic length and the number of branch terminals by Gö6976 treatment (Fig. 6G,H). By contrast, the number of primary dendrites was significantly increased in the presence of Gö6976 (control: 3.85±0.31, n=14; Gö6976: 6.42±0.58, n=12 at 90 hours; Fig. 6I). Time-lapse images revealed that the loss of primary stem dendrites in early stages was suppressed in Gö6976-treated cells (supplementary material Movie 4).

We evaluated time-dependent changes in the geometrical patterns of Purkinje cell dendrites by Sholl analysis (Sholl, 1953). In control cells, peaks of branch distribution were shifted distally as development proceeded, in concert with elongation and branching of dendritic terminals (Fig. 6J, top). Notably, the number of proximal branches around the soma gradually decreased during dendrite outgrowth. This could be accounted for either by elimination of proximal branches or by elongation of proximal segments. As elongation occurred exclusively at active growing terminals (Fig. 2), the clearance of proximal dendrites was likely to be due to branch retraction. Consistent with this prediction, reduction of the proximal intersections was not observed in Gö6976-treated neurons defective in branch retraction: new branches were added distally without changes in proximal branches (Fig. 6J, bottom). In addition, the distal shift of peak branch density was retarded in Gö6976-treated cells owing to slower elongation and branching.

We measured next the segment length by order of branches to compare further the arborization patterns of dendrites in the presence and absence of the inhibitor. Dendritic segments interconnected by branching nodes were numbered in centrifugal order (Fig. 1C, left). In control cells, the length of the first and second order segments progressively increased, whereas that of higher order segments were rather constant during development (Fig. 6K, top). Time-lapse imaging indicated that the apparent extension of proximal segments in control cells was due to contact-dependent retraction of proximal branches, leading to disappearance of the branching nodes and ligation of two sequential segments into a single long segment. By contrast, the length of proximal segments in inhibitor-treated cells remained constant and was comparable to higher order branches (Fig. 6K, bottom). Thus, contact-dependent elimination appears to preferentially reduce proximal branches and to contribute to the characteristic shape of Purkinje dendrite arbors, with long primary and secondary segments and short distal segments.

Involvement of PKCμ (PKD1) in dendrite retraction

To confirm PKC involvement in dendrite dynamics, we examined the effect of PKC activation with phorbol ester.

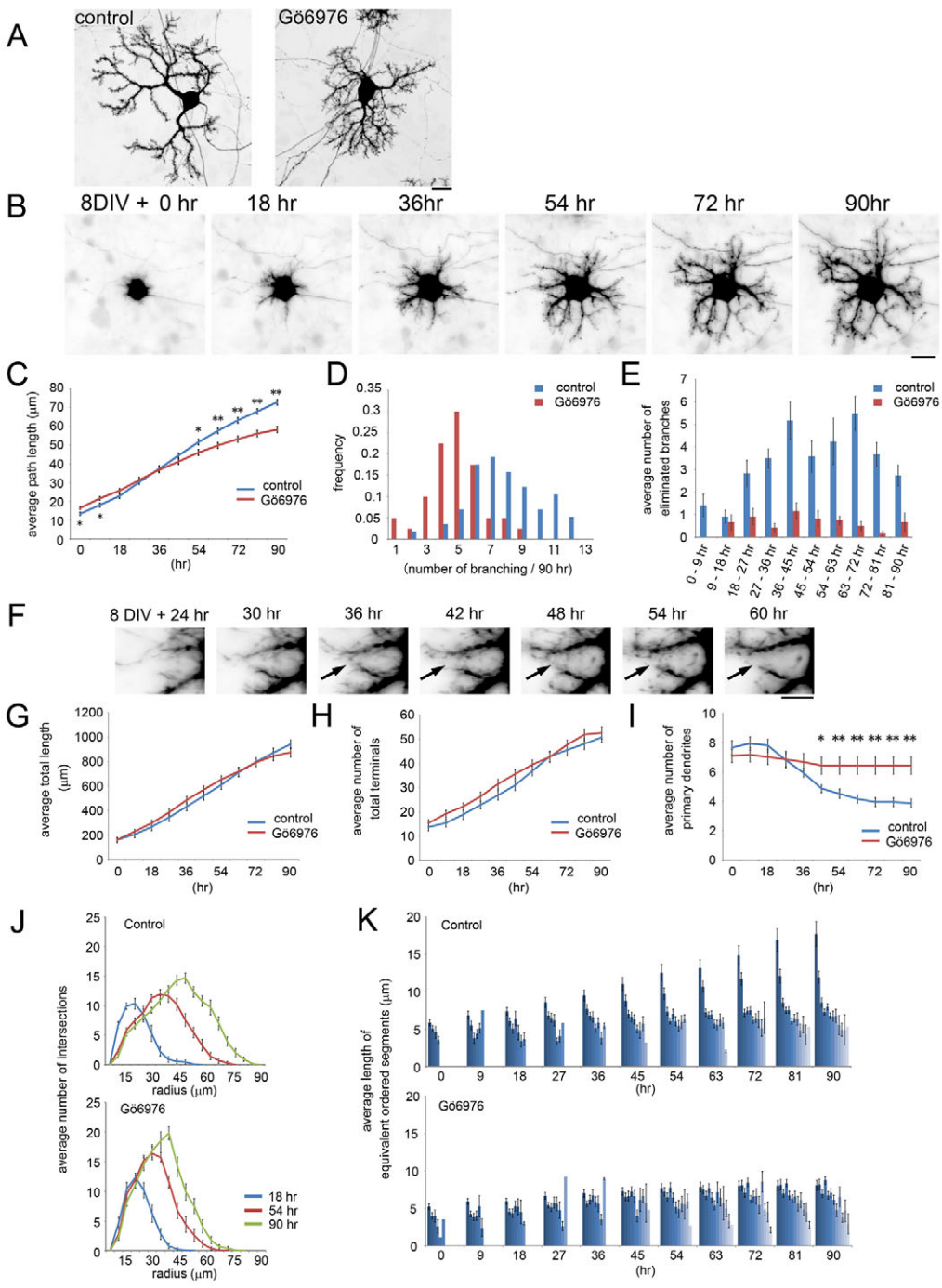

Fig. 6. PKC inhibition affects dynamics of dendrite growth. (**A**) Purkinje cells at 12 DIV grown with or without 100 nM Gö6976. (**B**) Time-lapse images of a Purkinje cell treated with Gö6976. (**C**) Average path length from the soma to growing terminals in control (blue) and inhibitor-treated (red) cells. The foremost growing terminal of each primary dendrite was selected for analyses. Control, *n*=13; Gö6976, *n*=12. (**D**) The distributions of cumulative counts of branching events per terminal over a 90-hour period with (red) or without (blue) Gö6976. (**E**) The number of eliminated branches per cell with (red) or without (blue) Gö6976. Events were counted after branch elimination was completed. (**F**) Contact-dependent retraction was suppressed in the presence of Gö6976. Filopodial protrusions in the distal tips that contacted a nearby dendrite were degraded (arrows) and the branch was stabilized in the proximity of the contacted dendrites. (**G-I**) Developmental changes in the total length (G), number of terminals (H) and number of primary dendrites (I) with (red) or without (blue) Gö6976. Control, *n*=13; Gö6976, *n*=12. (**J**) Sholl analysis of growing Purkinje cells in control (upper panel) and in Gö6976-treated (lower panel) cells. (**K**) Changes in the average length of equivalent ordered segments in control (upper panel; *n*=13) and in Gö6976-treated (lower panel; *n*=12) cells. Each bar represents mean ± s.e.m. of segment length (left: proximal; right: distal) at the indicated time points. **P*<0.05, ***P*<0.01. Scale bars: in A,B, 20 μm; in F, 10 μm.

Purkinje cells treated with 10 nM phorbol ester immediately withdrew growing dendrites proximally (supplementary material Movie 6). These results point to a role of PKC signaling in dendrite retraction.

In an attempt to identify the PKC subtype(s) involved in the dendrite retraction, we tested the effects of several PKC inhibitors with differential subtype specificities on the dendrite morphology. Among the five inhibitors examined, only Gö6976 treatment induced dendrites with crowded proximal segments (supplementary material Table S1). Comparison of subtype specificities highlighted PKCμ as a potential candidate molecule involved in dendrite retraction. PKCμ has recently been renamed protein kinase D1 (PKD1; Prkd1 – Mouse Genome Informatics) and is one of three isoforms: PKD1, PKD2 (Prkd2 – Mouse Genome Informatics) and PKCν (PKD3; Pkrd3 – Mouse Genome Informatics) (Rykx et al., 2003). We first confirmed by immunocytochemistry that all PKD isoforms were expressed in Purkinje cells as previously reported (Azoitei et al., 2011) (Allen Brain Atlas: http://mouse.brain-map.org). PKD1-3 exhibited overlapping but not identical subcellular localization (supplementary material Fig. S2): PKD1 and PKD2 localized at the Golgi apparatus in perinuclear regions and proximal dendrites, whereas PKD3 was enriched in the nucleus. Diffuse signals of PKD1 and PKD3 were also seen along dendrites. Transfected PKD1 preferentially localized to the cell periphery, including filopodia, and to cytoplasmic vesicles in Purkinje dendrites (supplementary material Fig. S2E).

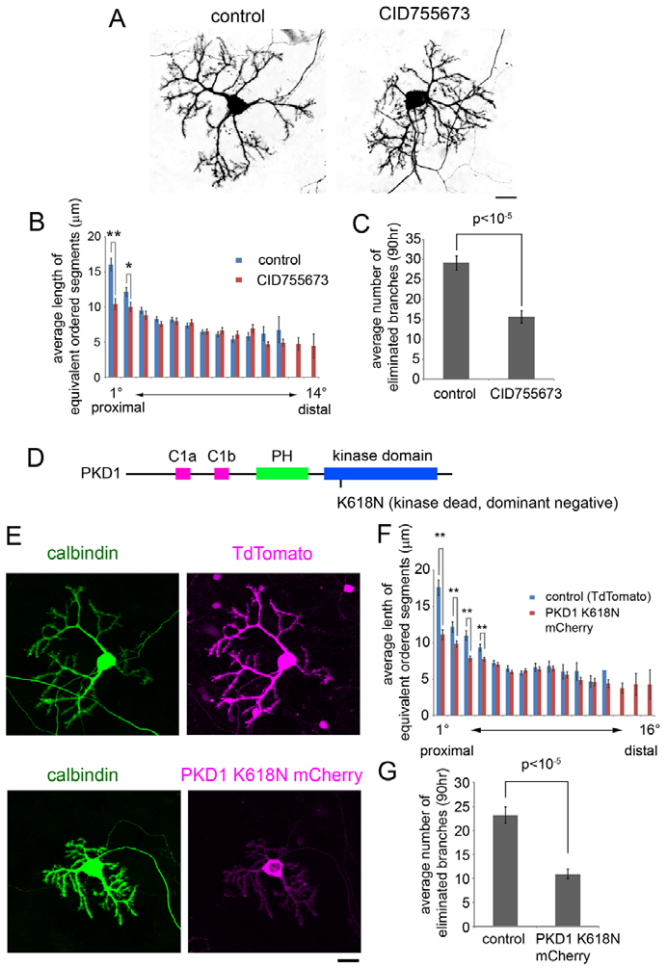

Fig. 7. Involvement of protein kinase D (PKD) in Purkinje cell dendrite morphogenesis. (**A**) Purkinje cells at 12 DIV grown in the presence and absence of 10 μM CID755673. (**B**) Average length of equivalent ordered segments in the cells cultured with (red) or without (blue) 10 μM CID755673. Control, *n*=25; CID755673, *n*=22. **P*<0.05, ***P*<0.01. (**C**) Average number of eliminated branches per cell with or without CID755673 over a 90-hour period. Control, *n*=26; CID755673, *n*=21. (**D**) Schematic of PKD1 structure. C1a and C1b, cysteine-rich domains that bind to diacylglycerol and phorbol ester; PH, pleckstrin homology domain. (**E**) Representative images of Purkinje cells at 11 DIV expressing TdTomato (upper) and PKD1 K618N-mCherry (lower). (**F**) Average length of equivalent ordered segments in cells transfected with TdTomato (blue; *n*=25) or PKD1 K618N (red; *n*=48). **P*<0.05, ***P*<0.01. (**G**) Average number of eliminated branches per cell over a 90-hour period of time-lapse observation in cells expressing TdTomato or PKD K618N-mCherry. TdTomato, *n*=14; PKD K618N mCherry, *n*=28. Error bars represent s.e.m. Scale bars: 20 μm.

To confirm the involvement of PKDs, we utilized CID755673, a potent and selective inhibitor of kinase activity of PKDs with minimal effect on classical PKCs (Sharlow et al., 2008). CID755673 induced complicated dendritic arbors with higher spatial density and with shorter proximal segments similar to those treated with Gö6976 (Fig. 7A,B). Neither total dendritic length (control: 1326±76 μm, *n*=25; CID755673: 1337±81 μm, *n*=22) nor the number of dendritic terminals (control: 79.4±5.6, *n*=25; CID755673: 86.4±5.7, *n*=22) was significantly affected in CID755673-treated cells. By contrast, CID755673 significantly suppressed dendrite retraction in time-lapse images (Fig. 7C). However, inhibition of dendritic retraction by CID755673 was less efficient than that induced by Gö6976 (number of eliminated dendrites: control: 29.2±1.8, *n*=26 versus CID755673: 15.6±1.5, *n*=21, $P<10^{-5}$; compared with control: 33.6±2.14, *n*=12 versus Gö6976: 6.1±1.5, *n*=12, $P<10^{-9}$). Incomplete suppression of branch retraction could imply that other PKC subtypes or kinases blocked by Gö6976 might regulate dendrite retraction in parallel with the PKD pathway. The contribution of PKD in dendrite retraction was validated further by genetic inhibition using a dominant-negative form of PKD1 (Fig. 7D). Overexpression of kinase-dead mutant PKD1 K618N is thought to block activities of all PKD isoforms to varying degrees (Rémillard-Labrosse et al., 2009). PKD1 K618N was transfected by nucleofection as it exceeded the limited insert size of the AAV vector. Similarly to CID755673, Purkinje cells expressing PKD1 K618N exhibited crowded dendrites with significantly shorter proximal segments compared with control cells expressing TdTomato (Fig. 7E,F). In time-lapse movies, retraction of growing dendrites was significantly inhibited in PKD1 K618N-expressing cells (Fig. 7G; supplementary material Movies 7, 8). Consistent with Gö6976 treatment, PKD1 K618N did not alter branching probability per unit length (control: 0.160±0.008 times/μm, *n*=25 dendrites from 12 cells; PKD1 K618N: 0.151±0.007 times /μm, *n*=49 dendrites from 26 cells; *P*=0.45), as it simultaneously lowered elongation speed (control: 0.53±0.02 μm/hour, *n*=25 dendrites from 12 cells; PKD1 K618N: 0.38±0.01 μm/hour, *n*=49 dendrites from 26 cells; $P<10^{-5}$) and branching frequency (control: 0.082±0.003 times/hour, *n*=25 dendrites from 12 cells; PKD1 K618N: 0.057±0.003, *n*=49 dendrites from 26 cells; $P<10^{-5}$). Taking these data together, we conclude that dendritic retraction in growing Purkinje cells is at least partly mediated by PKD activity.

Computer-assisted simulation of dendrite formation in cultured Purkinje cells

The results described above suggest the important contribution of contact-dependent retraction to Purkinje cell morphogenesis. In order to support this view, we performed a computer-assisted simulation of dendrite growth using experimental values of a parameter set obtained from time-lapse images of live Purkinje cells. The initial dendrites emerged from random positions on the perimeter of a soma. The constant elongation of dendritic terminals was recapitulated by the addition of one unit fragment per 3 hours (=1 step in simulation) at the terminal of the dendrites (supplementary material Fig. S3). Dichotomous branching was reproduced by the addition of two unit fragments to the dendritic terminal at a mean bifurcation angle of 65°. The branching was set to take place stochastically at an average rate of 0.26 times/3 hours. In the model of control cells (condition 1), a branch segment was eliminated at 21 hours after the growing tip contacted other branches. In the model of retraction-deficient cells (condition 3), branch growth was arrested by contacts between branches. Other parameters, including elongation and branching, were the same in control and retraction-deficient cells. Figure 8A shows representative images of growing cells in the models. The apparent shapes of the control and retraction-deficient cells were strikingly reminiscent of the live control and Gö6976-treated Purkinje cells, respectively. Early loss of primary dendrites took place only in control cells with contact-dependent retraction (condition 1 in Fig. 8A,B; supplementary material Movie 9). By contrast, excess branches increasingly accumulated in retraction-deficient cells (condition 3 in Fig. 8A; supplementary material Movie 11).

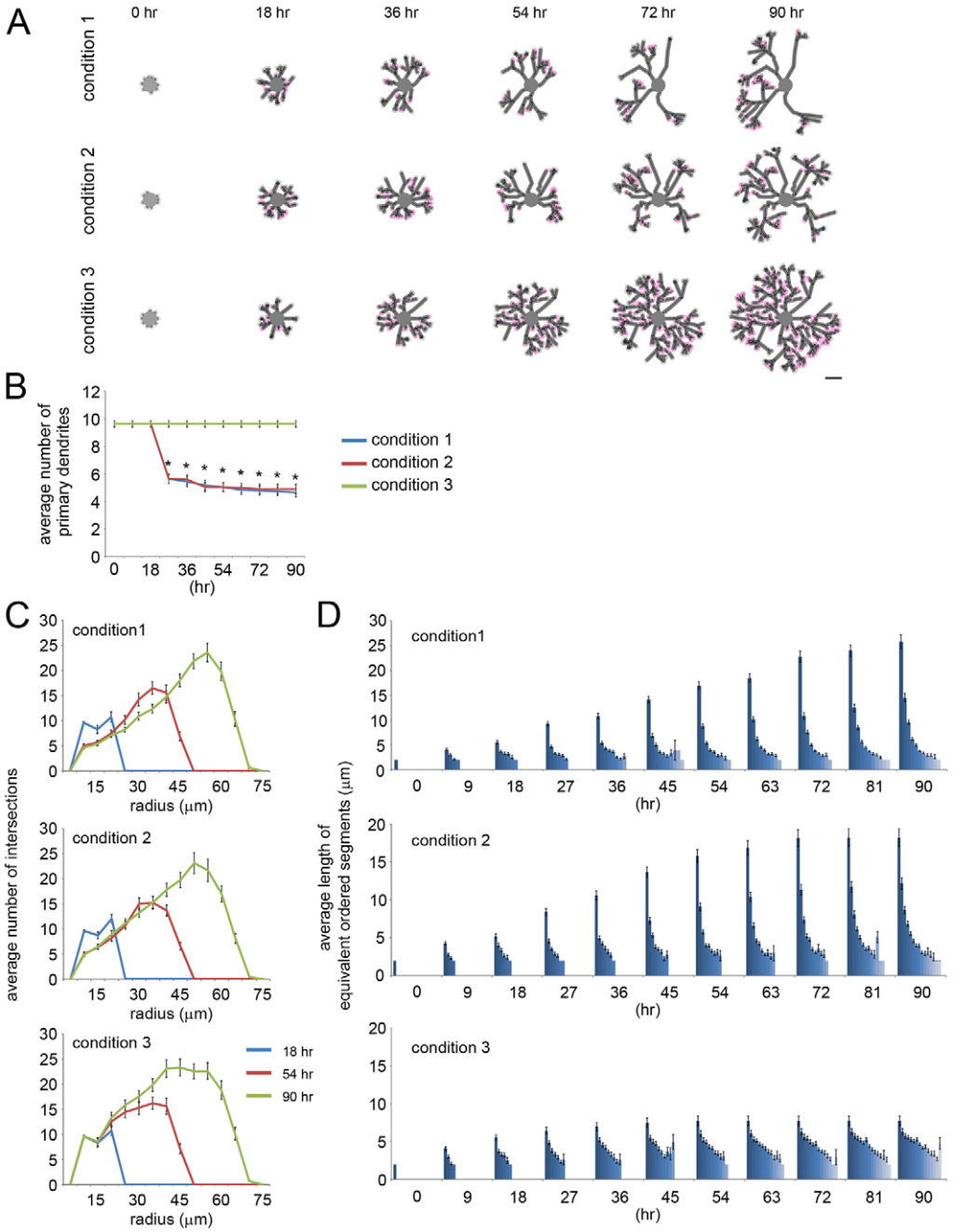

Fig. 8. Reconstruction of dendrite dynamics in silico. (**A**) Representative images of dendrite growth in simulated Purkinje cells. (**B**) Developmental changes in the mean number of primary dendrites in the simulated cells in conditions 1-3 (one-way ANOVA, post-hoc Tukey test, **P*<0.01, *n*=20 for each condition). (**C**,**D**) Sholl analysis (C) and the average length of equivalent ordered segments (D) in the simulated cells in conditions 1-3 (*n*=20 for each condition). Each bar in D represents mean ± s.e.m. of segment length (left: proximal; right: distal) at the indicated time points.

Notably, the early contact-independent retraction of stem dendrites was not included in the parameter sets, indicating that its contribution is dispensable for the reduction of the primary dendrite number. Sholl analyses indicated that developmental changes in dendrite configuration in the model cells remarkably paralleled those in live cells (Fig. 8C). Furthermore, time-dependent elongation of the proximal segments was seen in the model control cell, whereas it was abrogated in the retraction-deficient cell (Fig. 8D, compare conditions 1 and 3). By contrast, other changes seen in Gö6976-treated cells, including elongation speed and branching probability, had little effect on spatial distribution of dendrites except for an overall reduction in the arbor size (supplementary material Fig. S4). Specifically, the gradual elongation of the first-order segment was hardly affected by the perturbations in the elongation speed and/or branching probability in the model, unlike in the retraction-deficient conditions. These results indicate that contact-dependent retraction of branches is the major cause for the apparent extension of proximal segments and reduced complexity in the perisomal region.

By contrast, the segment length was progressively shortened from the proximal to distal segments in condition 1, whereas it plateaued in the higher order segments in real cells (Fig. 6K, Fig. 8D). We attributed this incompatibility to the oversimplified conditions of retraction in the model, and subsequently accounted for the time-dependent mode transition of the contact-induced response from branch retraction to branch stalling, as was observed in real cells (Fig. 4D). Under these conditions, the distribution of segment length in the modified model of control cells was much more similar to the live control cells (condition 2 in Fig. 8A,D; supplementary material Movie 10).

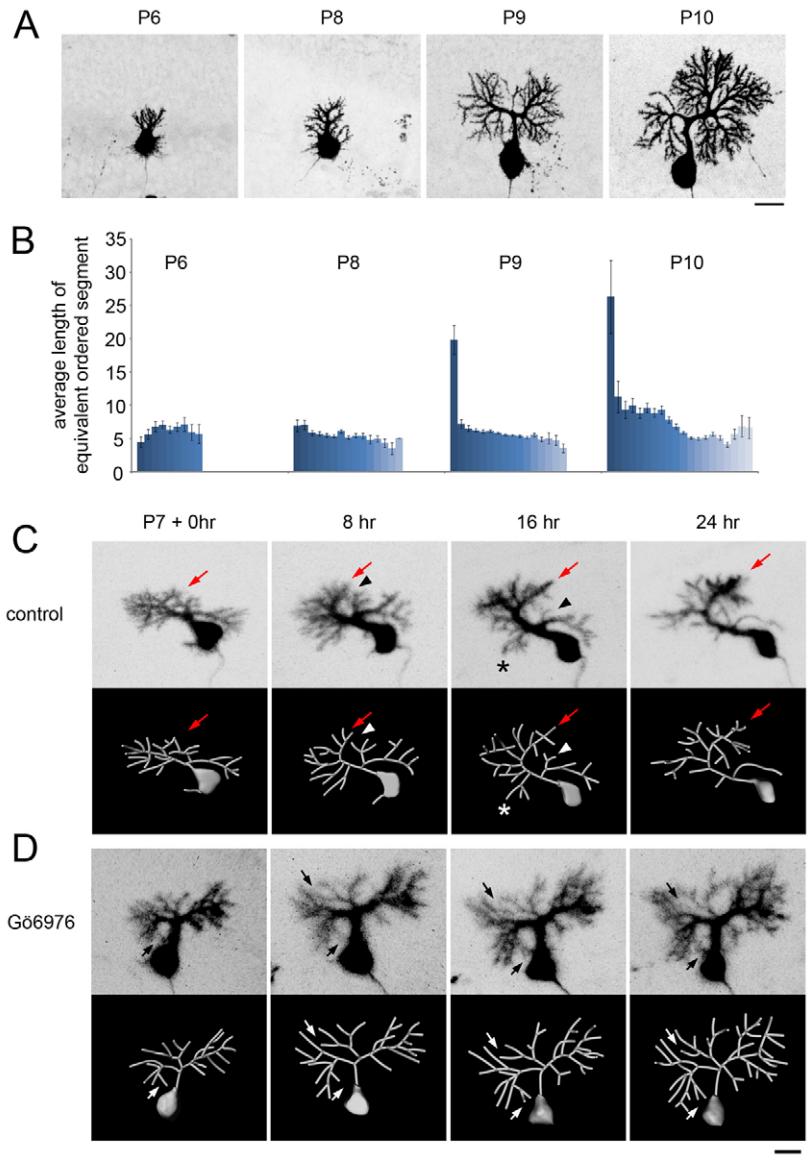

Fig. 9. Dendrite development in vivo and in slice culture. (**A**) Representative images of GFP-labeled Purkinje cells at the indicated ages. (**B**) The mean length of equivalent ordered segments of growing Purkinje cell dendrites. Each bar represents mean ± s.e.m. of segment length (left: proximal; right: distal) at the indicated ages (P6, *n*=12 cells; P8, *n*=26 cells; P9, *n*=27 cells; P10, *n*=22 cells). (**C**) Time-lapse observation of Purkinje cell development at 8-hour intervals in slice culture without Gö6976. Elongation and branching (red arrows) and retraction triggered by dendro-dendritic contacts (arrowheads) were observed. Some lateral branches (asterisks) were also retracted seemingly after contacts with neighboring cells. (**D**) The time-lapse observation of a Purkinje cell treated with Gö6976. Dendro-dendritic contacts failed to induce branch retraction (arrows). Scale bars: 20 μm.

Together, these results support the notion that the simple set of parameters of dynamics that include elongation, branching and elimination extracted from real cells are sufficient for modeling some morphometric characteristics of growing Purkinje dendrites in culture. Moreover, contact-dependent repulsion of dendritic branches was found to be crucial for the spatial distribution of dendrite branches, with long proximal segments and short higher-ordered segments, in addition to their non-overlapping arrangement.

Contact-dependent branch elimination in Purkinje cells in the cerebellar cortex

During postnatal development, the first dendritic segments in Purkinje cells are gradually elongated to a greater degree than higher order segments (Fig. 1, Fig. 9A,B). To confirm the contribution of branch elimination to dendrite configuration in vivo, we performed time-lapse observation using an organotypic culture in which the cortical cytoarchitecture of the cerebellum was at least partly retained. Extensive elongation and branching of dendrite tips were observed in slice culture (Fig. 9C, arrows). Retraction of growing branches was also evident and appeared to follow contacts with other branches of the same or adjacent cells (Fig. 9C, arrowheads and asterisks). Retraction of proximal branches caused elimination of the branching nodes and increased the length of the proximal segments. Such contact-dependent retraction was repressed by the application of Gö6976 in slice culture, consistent with the data using dissociation cultures (Fig. 9D, arrows). These data support the notion that the contact-dependent retraction plays a pivotal role in spatial arrangement of Purkinje cell dendrites.

DISCUSSION

Basic dynamics of Purkinje cell dendrite outgrowth

Quantitative assessment of dendrite outgrowth in cultured Purkinje cells by long-term time-lapse imaging revealed that the essential rules of dendrite arborization are a combination of relatively simple dynamics despite of their intricate appearance: Our experimental observations agreed with earlier predictions using fixed Golgi-stained cells (Hollingworth and Berry, 1975; Sadler and Berry, 1989). The former study generated possible topological patterns of dendrites by computer simulations assembling several putative

branching rules. Of those, the dendrite pattern formed by stochastic addition of branches to dendritic terminals was similar to the morphology of real Purkinje cell dendrites. Consistently, direct observation of growing dendrites in the present study indicate that the basic frameworks of dendrites are constructed by constant elongation and random dichotomous branching at active sites near the termini of dendrites. This is in contrast to hippocampal pyramidal cells, which are known to sprout collateral branches from the shaft of dendrites (Dailey and Smith, 1996). Thus, dendrite dynamics vary by neuronal species with distinct morphology (Hattori et al., 2007; Jinushi-Nakao et al., 2007).

Time-lapse imaging also revealed dendrite repulsion, including retraction and stalling, which were induced by contacts or tight apposition with neighboring dendrites. Dendritic repulsion was a two-step process seen in early phases of dendrite growth: the dendritic tips immediately stalled upon collision with nearby dendrite(s), and they were retracted by one or two segments in the 20 hours after collision. Responsiveness to the retraction-inducing signal might decay during dendrite differentiation, as increasing numbers of branches were stalled and stabilized rather than retracted after dendro-dendritic collision in the late phase of dendrite outgrowth. We demonstrated that the contact-induced retraction is regulated by PKD kinase activity. Contact-independent retraction of emerging primary dendritic processes in earlier stages were also suppressed by inhibition of PKD, suggesting that branch retraction mechanisms converge at the level of PKD regardless of initiation cues.

The PKD family controls a variety of cellular functions, including remodeling of actin filaments (Eiseler et al., 2010; Spratley et al., 2011), receptor recycling (Woods et al., 2004; di Blasio et al., 2010), vesicle transport at the trans-Golgi network (Hausser et al., 2005) and neuronal polarization (Bisbal et al., 2008; Yin et al., 2008). In hippocampal neurons, suppression of PKD activity has been shown to cause a significant decrease in dendritic size and complexity, presumably owing to a deficit in secretory transport in dendrites (Horton et al., 2005; Czöndör et al., 2009). We observed overlapping but distinct subcellular localization of PKD isoforms in the Golgi apparatus, nucleus, dendritic periphery and cytoplasm in Purkinje cells. It is thus plausible that PKD activity affects multiple branch dynamics, including dendrite retraction and elongation, via regulation of different cellular contexts. Candidate upstream mediators of PKD during contact-dependent dendrite retractions would be homophilic adhesion molecules, such as Dscam, Turtle and Cadherin superfamily molecules Flamingo/Celsr 1,2,3, that are responsible for the recognition of homotypic interaction of dendrites (Kimura et al., 2006; Fuerst et al., 2008; Fuerst et al., 2009; Long et al., 2009). Precise molecular mechanisms underlying the contact-dependent repulsion and other branch dynamics are an important direction for future studies.

Reconstruction of dendrite outgrowth in computer simulations based on time-lapse observations

In contrast to previous simulation studies aiming to define the elementary rules for dendrite growth using hypothetical parameter sets (Hollingworth and Berry, 1975; van Pelt, 1997; van Pelt and Uylings, 2002; Luczak, 2006; Sugimura et al., 2007; Shimono et al., 2010), we adopted the actual values of dynamic parameters obtained by live imaging, and reproduced the deployment of dendritic arbors of real Purkinje cells. Our time-lapse images proved that proximal segments gradually increased in length, whereas higher ordered segments remained constant. Consistent with the prediction of earlier anatomical studies (Berry and Bradley, 1976b), the present live imaging demonstrates that retraction of proximal branches is induced by dendro-dendritic contacts in Purkinje cells. Here, the computer simulation provides a powerful approach to dissect the relative impact of each aspect of dynamics in appropriate dendrite morphogenesis: the contact-induced branch repulsion was confirmed to be crucial for the spatial disposition of dendrites, whereas elongation speed, branching probability of growing terminals and contact-independent retraction had only minor effects. Thus, time-lapse observation combined with numerical simulations enabled us to extract the important dynamic parameters for dendrite morphogenesis by means of a recursive method.

Physiological implications of contact-dependent retraction and stalling

Purkinje cells elaborate numerous dendritic branches in flat parasagittal planes that cover their receptive fields with minimal overlaps. Self-repulsive properties ensure the dendritic tiling for complete and non-redundant coverage of the receptive field in invertebrate sensory neurons and mammalian retinal ganglion cells (Wässle et al., 1981; Perry and Linden, 1982; Grueber and Truman, 1999; Grueber et al., 2002; Sugimura et al., 2003). We assume that, among repulsive reactions in the Purkinje cell, the contact-dependent retraction in earlier stages contributes to the segment distribution in the proximal dendrites, whereas the contact-dependent stalling ensures the non-overlapping arrays of distal branches in the same cell (self-avoidance) and between neighboring Purkinje cells (regular alignment or tiling).

Comparison of in vivo and in vitro Purkinje cells

Despite many morphological similarities between Purkinje cell dendrites in dissociation culture and in vivo, there are a number of significant differences, including the small arboreal size and the number of the primary dendrites. Small arboreal size and complexity are probably due to lack or shortage of trophic and structural support from neighboring cells, including granule cells and inhibitory interneurons (Baptista et al., 1994; Altman and Bayer, 1997; Kawaguchi et al., 2010). Purkinje cells in vivo retain a single primary dendrite from numerous immature primary dendrites in the second postnatal week. The reduction of primary dendrites was recapitulated in dissociation culture, but most Purkinje cells retained three or four primary dendrites at fully developed stages in culture. As Purkinje cells are sparsely distributed in dissociated culture, retraction of primary dendrites was induced mostly by dendro-dendritic contacts in the same cell. By contrast, Purkinje cell dendrites in vivo are densely filled in the molecular layer, and most of the original primary dendrites are likely to be eliminated by frequent contacts with dendrites of the same and adjacent cells. Three-dimensional computer simulation following detailed in vivo analyses of developing Purkinje cells would be the next step for a better understanding of Purkinje cell development.

The present combinatorial approach using time-lapse imaging and computer simulations will be of use in searching for fundamentals of various dendrite patterns. It will also help to clarify the specific actions of functional molecules in dendrite dynamics and how they orchestrate dendrite shape.

Acknowledgements
We thank Drs J. Hejna and C. Yokoyama for invaluable advice for the manuscript.

Funding
This work was supported by the Funding Program for Next Generation World-Leading Researchers (NEXT Program) of the Government of Japan; a Grant-in-Aid for Scientific Research on Innovative Areas 'Mesoscopic Neurocircuitry' [22115008 and 23115102]; and a grant from Brain Science Foundation. The iCeMS is supported by World Premier International Research Center Initiative (WPI), MEXT, Japan. Deposited in PMC for immediate release.

Competing interests statement
The authors declare no competing financial interests.

Supplementary material
Supplementary material available online at
http://dev.biologists.org/lookup/suppl/doi:10.1242/dev.081315/-/DC1

References
Altman, J. and Bayer, S. A. (1997). *Development of the Cerebellar System*. Florida, CA: CRC Press.
Azoitei, N., Kleger, A., Schoo, N., Thal, D. R., Brunner, C., Pusapati, G. V., Filatova, A., Genze, F., Möller, P., Acker, T. et al. (2011). Protein kinase D2 is a novel regulator of glioblastoma growth and tumor formation. *Neuro-oncol.* **13**, 710-724.
Baptista, C. A., Hatten, M. E., Blazeski, R. and Mason, C. A. (1994). Cell-cell interactions influence survival and differentiation of purified purkinje cells in vitro. *Neuron* **12**, 243-260.
Berry, M. and Bradley, P. (1976a). The growth of the dendritic trees of Purkinje cells in irradiated agranular cerebellar cortex. *Brain Res.* **116**, 361-387.
Berry, M. and Bradley, P. (1976b). The growth of the dendritic trees of Purkinje cells in the cerebellum of the rat. *Brain Res.* **112**, 1-35.
Berry, M. and Flinn, R. (1984). Vertex analysis of Purkinje cell dendritic trees in the cerebellum of the rat. *Proc. R. Soc. Lond. B Biol. Sci.* **221**, 321-348.
Berry, M., Hollingworth, T., Flinn, R. M. and Anderson, E. M. (1972). The growth of Purkinje cell dendrites of the rat-a quantitative study. *J. Anat.* **111**, 491-493.
Bisbal, M., Conde, C., Donoso, M., Bollati, F., Sesma, J., Quiroga, S., Diaz Anel, A., Malhotra, V., Marzolo, M. P. and Caceres, A. (2008). Protein kinase d regulates trafficking of dendritic membrane proteins in developing neurons. *J. Neurosci.* **28**, 9297-9308.
Branco, T. and Häusser, M. (2010). The single dendritic branch as a fundamental functional unit in the nervous system. *Curr. Opin. Neurobiol.* **20**, 494-502.
Calvet, M. C., Calvet, J. and Camacho-Garcia, R. (1985). The Purkinje cell dendritic tree: a computer-aided study of its development in the cat and in culture. *Brain Res.* **331**, 235-250.
Czöndör, K., Ellwanger, K., Fuchs, Y. F., Lutz, S., Gulyás, M., Mansuy, I. M., Hausser, A., Pfizenmaier, K. and Schlett, K. (2009). Protein kinase D controls the integrity of Golgi apparatus and the maintenance of dendritic arborization in hippocampal neurons. *Mol. Biol. Cell* **20**, 2108-2120.
Dailey, M. E. and Smith, S. J. (1996). The dynamics of dendritic structure in developing hippocampal slices. *J. Neurosci.* **16**, 2983-2994.
Di Blasio, L., Droetto, S., Norman, J., Bussolino, F. and Primo, L. (2010). Protein kinase D1 regulates VEGF-A-induced alphavbeta3 integrin trafficking and endothelial cell migration. *Traffic* **11**, 1107-1118.
Eiseler, T., Hausser, A., De Kimpe, L., Van Lint, J. and Pfizenmaier, K. (2010). Protein kinase D controls actin polymerization and cell motility through phosphorylation of cortactin. *J. Biol. Chem.* **285**, 18672-18683.
Emoto, K., He, Y., Ye, B., Grueber, W. B., Adler, P. N., Jan, L. Y. and Jan, Y. N. (2004). Control of dendritic branching and tiling by the Tricornered-kinase/Furry signaling pathway in Drosophila sensory neurons. *Cell* **119**, 245-256.
Emoto, K., Parrish, J. Z., Jan, L. Y. and Jan, Y. N. (2006). The tumour suppressor Hippo acts with the NDR kinases in dendritic tiling and maintenance. *Nature* **443**, 210-213.
Fuerst, P. G., Koizumi, A., Masland, R. H. and Burgess, R. W. (2008). Neurite arborization and mosaic spacing in the mouse retina require DSCAM. *Nature* **451**, 470-474.
Fuerst, P. G., Bruce, F., Tian, M., Wei, W., Elstrott, J., Feller, M. B., Erskine, L., Singer, J. H. and Burgess, R. W. (2009). DSCAM and DSCAML1 function in self-avoidance in multiple cell types in the developing mouse retina. *Neuron* **64**, 484-497.
Gan, W. B. and Macagno, E. R. (1995). Interactions between segmental homologs and between isoneuronal branches guide the formation of sensory terminal fields. *J. Neurosci.* **15**, 3243-3253.
Gao, F. B. (2007). Molecular and cellular mechanisms of dendritic morphogenesis. *Curr. Opin. Neurobiol.* **17**, 525-532.
Grueber, W. B. and Truman, J. W. (1999). Development and organization of a nitric-oxide-sensitive peripheral neural plexus in larvae of the moth, Manduca sexta. *J. Comp. Neurol.* **404**, 127-141.
Grueber, W. B., Jan, L. Y. and Jan, Y. N. (2002). Tiling of the Drosophila epidermis by multidendritic sensory neurons. *Development* **129**, 2867-2878.
Grueber, W. B., Jan, L. Y. and Jan, Y. N. (2003). Different levels of the homeodomain protein cut regulate distinct dendrite branching patterns of Drosophila multidendritic neurons. *Cell* **112**, 805-818.
Gschwendt, M., Dieterich, S., Rennecke, J., Kittstein, W., Mueller, H. J. and Johannes, F. J. (1996). Inhibition of protein kinase C mu by various inhibitors. Differentiation from protein kinase c isoenzymes. *FEBS Lett.* **392**, 77-80.
Han, C., Wang, D., Soba, P., Zhu, S., Lin, X., Jan, L. Y. and Jan, Y. N. (2012). Integrins regulate repulsion-mediated dendritic patterning of drosophila sensory neurons by restricting dendrites in a 2D space. *Neuron* **73**, 64-78.
Hattori, Y., Sugimura, K. and Uemura, T. (2007). Selective expression of Knot/Collier, a transcriptional regulator of the EBF/Olf-1 family, endows the Drosophila sensory system with neuronal class-specific elaborated dendritic patterns. *Genes Cells* **12**, 1011-1022.
Hausser, A., Storz, P., Märtens, S., Link, G., Toker, A. and Pfizenmaier, K. (2005). Protein kinase D regulates vesicular transport by phosphorylating and activating phosphatidylinositol-4 kinase IIIbeta at the Golgi complex. *Nat. Cell Biol.* **7**, 880-886.
Hirai, H. (2008). Progress in transduction of cerebellar Purkinje cells in vivo using viral vectors. *Cerebellum* **7**, 273-278.
Hirai, H. and Launey, T. (2000). The regulatory connection between the activity of granule cell NMDA receptors and dendritic differentiation of cerebellar Purkinje cells. *J. Neurosci.* **20**, 5217-5224.
Hollingworth, T. and Berry, M. (1975). Network analysis of dendritic fields of pyramidal cells in neocortex and Purkinje cells in the cerebellum of the rat. *Philos. Trans. R. Soc. Lond. B Biol. Sci.* **270**, 227-264.
Horton, A. C., Rácz, B., Monson, E. E., Lin, A. L., Weinberg, R. J. and Ehlers, M. D. (2005). Polarized secretory trafficking directs cargo for asymmetric dendrite growth and morphogenesis. *Neuron* **48**, 757-771.
Jan, Y. N. and Jan, L. Y. (2010). Branching out: mechanisms of dendritic arborization. *Nat. Rev. Neurosci.* **11**, 316-328.
Jinushi-Nakao, S., Arvind, R., Amikura, R., Kinameri, E., Liu, A. W. and Moore, A. W. (2007). Knot/Collier and cut control different aspects of dendrite cytoskeleton and synergize to define final arbor shape. *Neuron* **56**, 963-978.
Jirousek, M. R., Gillig, J. R., Gonzalez, C. M., Heath, W. F., McDonald, J. H., 3rd, Neel, D. A., Rito, C. J., Singh, U., Stramm, L. E., Melikian-Badalian, A. et al. (1996). (S)-13-[(dimethylamino)methyl]-10,11,14,15-tetrahydro-4,9:16,21-dimetheno-1H, 13H-dibenzo[e,k]pyrrolo[3,4-h][1,4,13]oxadiazacyclohexadecene-1,3(2H)-d ione (LY333531) and related analogues: isozyme selective inhibitors of protein kinase C beta. *J. Med. Chem.* **39**, 2664-2671.
Kaneko, M., Yamaguchi, K., Eiraku, M., Sato, M., Takata, N., Kiyohara, Y., Mishina, M., Hirase, H., Hashikawa, T. and Kengaku, M. (2011). Remodeling of monoplanar Purkinje cell dendrites during cerebellar circuit formation. *PLoS ONE* **6**, e20108.
Kapfhammer, J. P. (2004). Cellular and molecular control of dendritic growth and development of cerebellar Purkinje cells. *Prog. Histochem. Cytochem.* **39**, 131-182.
Kawaguchi, K., Habara, T., Terashima, T. and Kikkawa, S. (2010). GABA modulates development of cerebellar Purkinje cell dendrites under control of endocannabinoid signaling. *J. Neurochem.* **114**, 627-638.
Kim, M. E., Shrestha, B. R., Blazeski, R., Mason, C. A. and Grueber, W. B. (2012). Integrins establish dendrite-substrate relationships that promote dendritic self-avoidance and patterning in drosophila sensory neurons. *Neuron* **73**, 79-91.
Kimura, H., Usui, T., Tsubouchi, A. and Uemura, T. (2006). Potential dual molecular interaction of the Drosophila 7-pass transmembrane cadherin Flamingo in dendritic morphogenesis. *J. Cell Sci.* **119**, 1118-1129.
Li, J., Gu, X., Ma, Y., Calicchio, M. L., Kong, D., Teng, Y. D., Yu, L., Crain, A. M., Vartanian, T. K., Pasqualini, R. et al. (2010). Nna1 mediates Purkinje cell dendritic development via lysyl oxidase propeptide and NF-κB signaling. *Neuron* **68**, 45-60.
London, M. and Häusser, M. (2005). Dendritic computation. *Annu. Rev. Neurosci.* **28**, 503-532.
Long, H., Ou, Y., Rao, Y. and van Meyel, D. J. (2009). Dendrite branching and self-avoidance are controlled by Turtle, a conserved IgSF protein in Drosophila. *Development* **136**, 3475-3484.
Lordkipanidze, T. and Dunaevsky, A. (2005). Purkinje cell dendrites grow in alignment with Bergmann glia. *Glia* **51**, 229-234.
Luczak, A. (2006). Spatial embedding of neuronal trees modeled by diffusive growth. *J. Neurosci. Methods* **157**, 132-141.
Marte, B. M., Meyer, T., Stabel, S., Standke, G. J., Jaken, S., Fabbro, D. and Hynes, N. E. (1994). Protein kinase C and mammary cell differentiation: involvement of protein kinase C alpha in the induction of beta-casein expression. *Cell Growth Differ.* **5**, 239-247.
Martiny-Baron, G., Kazanietz, M. G., Mischak, H., Blumberg, P. M., Kochs, G., Hug, H., Marme, D. and Schachtele, C. (1993). Selective inhibition of protein kinase C isozymes by the indolocarbazole Go 6976. *J. Biol. Chem.* **268**, 9194-9197.
McKay, B. E. and Turner, R. W. (2005). Physiological and morphological development of the rat cerebellar Purkinje cell. *J. Physiol.* **567**, 829-850.

Metzger, F. and Kapfhammer, J. P. (2003). Protein kinase C: its role in activity-dependent Purkinje cell dendritic development and plasticity. *Cerebellum* **2**, 206-214.
Mori, M. and Matsushima, T. (2002). Post-hatch development of dendritic arborization in cerebellar Purkinje neurons of quail chicks: a morphometric study. *Neurosci. Lett.* **329**, 73-76.
Mumm, J. S., Williams, P. R., Godinho, L., Koerber, A., Pittman, A. J., Roeser, T., Chien, C. B., Baier, H. and Wong, R. O. (2006). In vivo imaging reveals dendritic targeting of laminated afferents by zebrafish retinal ganglion cells. *Neuron* **52**, 609-621.
Napper, R. M. and Harvey, R. J. (1988). Number of parallel fiber synapses on an individual Purkinje cell in the cerebellum of the rat. *J. Comp. Neurol.* **274**, 168-177.
Niwa, H., Yamamura, K. and Miyazaki, J. (1991). Efficient selection for high-expression transfectants with a novel eukaryotic vector. *Gene* **108**, 193-199.
Ohkawa, N., Fujitani, K., Tokunaga, E., Furuya, S. and Inokuchi, K. (2007). The microtubule destabilizer stathmin mediates the development of dendritic arbors in neuronal cells. *J. Cell Sci.* **120**, 1447-1456.
Parrish, J. Z., Emoto, K., Kim, M. D. and Jan, Y. N. (2007). Mechanisms that regulate establishment, maintenance, and remodeling of dendritic fields. *Annu. Rev. Neurosci.* **30**, 399-423.
Perry, V. H. and Linden, R. (1982). Evidence for dendritic competition in the developing retina. *Nature* **297**, 683-685.
Portera-Cailliau, C., Pan, D. T. and Yuste, R. (2003). Activity-regulated dynamic behavior of early dendritic protrusions: evidence for different types of dendritic filopodia. *J. Neurosci.* **23**, 7129-7142.
Ramon y Cajal, S. (1911). *Histology of the Nervous System of Man and Vertebrates* (Translated from the French). Oxford, UK: Oxford University Press.
Rémillard-Labrosse, G., Mihai, C., Duron, J., Guay, G. and Lippé, R. (2009). Protein kinase D-dependent trafficking of the large Herpes simplex virus type 1 capsids from the TGN to plasma membrane. *Traffic* **10**, 1074-1083.
Rykx, A., De Kimpe, L., Mikhalap, S., Vantus, T., Seufferlein, T., Vandenheede, J. R. and Van Lint, J. (2003). Protein kinase D: a family affair. *FEBS Lett.* **546**, 81-86.
Sadler, M. and Berry, M. (1989). Topological link-vertex analysis of the growth of Purkinje cell dendritic trees in normal, reeler, and weaver mice. *J. Comp. Neurol.* **289**, 260-283.
Sharlow, E. R., Giridhar, K. V., LaValle, C. R., Chen, J., Leimgruber, S., Barrett, R., Bravo-Altamirano, K., Wipf, P., Lazo, J. S. and Wang, Q. J. (2008). Potent and selective disruption of protein kinase D functionality by a benzoxoloazepinolone. *J. Biol. Chem.* **283**, 33516-33526.
Shima, Y., Kengaku, M., Hirano, T., Takeichi, M. and Uemura, T. (2004). Regulation of dendritic maintenance and growth by a mammalian 7-pass transmembrane cadherin. *Dev. Cell* **7**, 205-216.
Shimono, K., Sugimura, K., Kengaku, M., Uemura, T. and Mochizuki, A. (2010). Computational modeling of dendritic tiling by diffusible extracellular suppressor. *Genes Cells* **15**, 137-149.
Sholl, D. A. (1953). Dendritic organization in the neurons of the visual and motor cortices of the cat. *J. Anat.* **87**, 387-406.
Sotelo, C. and Dusart, I. (2009). Intrinsic versus extrinsic determinants during the development of Purkinje cell dendrites. *Neuroscience* **162**, 589-600.
Spratley, S. J., Bastea, L. I., Döppler, H., Mizuno, K. and Storz, P. (2011). Protein kinase D regulates cofilin activity through p21-activated kinase 4. *J. Biol. Chem.* **286**, 34254-34261.
Sugimura, K., Yamamoto, M., Niwa, R., Satoh, D., Goto, S., Taniguchi, M., Hayashi, S. and Uemura, T. (2003). Distinct developmental modes and lesion-induced reactions of dendrites of two classes of Drosophila sensory neurons. *J. Neurosci.* **23**, 3752-3760.
Sugimura, K., Shimono, K., Uemura, T. and Mochizuki, A. (2007). Self-organizing mechanism for development of space-filling neuronal dendrites. *PLoS Comput. Biol.* **3**, e212.
Tanabe, K., Kani, S., Shimizu, T., Bae, Y. K., Abe, T. and Hibi, M. (2010). Atypical protein kinase C regulates primary dendrite specification of cerebellar Purkinje cells by localizing Golgi apparatus. *J. Neurosci.* **30**, 16983-16992.
Tanaka, M. (2009). Dendrite formation of cerebellar Purkinje cells. *Neurochem. Res.* **34**, 2078-2088.
Tanaka, M., Yanagawa, Y., Obata, K. and Marunouchi, T. (2006). Dendritic morphogenesis of cerebellar Purkinje cells through extension and retraction revealed by long-term tracking of living cells in vitro. *Neuroscience* **141**, 663-674.
van Pelt, J. (1997). Effect of pruning on dendritic tree topology. *J. Theor. Biol.* **186**, 17-32.
van Pelt, J. and Uylings, H. B. (2002). Branching rates and growth functions in the outgrowth of dendritic branching patterns. *Network* **13**, 261-281.
van Pelt, J., Graham, B. and Uylings, H. (2003). Formation of dendritic branching patterns. In *Modeling Neural Development* (ed. A. Van Ooyan). Cambridge, MA: The MIT Press.
Wagner, W., Brenowitz, S. D. and Hammer, J. A., 3rd (2011). Myosin-Va transports the endoplasmic reticulum into the dendritic spines of Purkinje neurons. *Nat. Cell Biol.* **13**, 40-48.
Wässle, H., Peichl, L. and Boycott, B. B. (1981). Dendritic territories of cat retinal ganglion cells. *Nature* **292**, 344-345.
Whitford, K. L., Dijkhuizen, P., Polleux, F. and Ghosh, A. (2002). Molecular control of cortical dendrite development. *Annu. Rev. Neurosci.* **25**, 127-149.
Wilkinson, S. E., Parker, P. J. and Nixon, J. S. (1993). Isoenzyme specificity of bisindolylmaleimides, selective inhibitors of protein kinase C. *Biochem. J.* **294**, 335-337.
Williams, D. W. and Truman, J. W. (2004). Mechanisms of dendritic elaboration of sensory neurons in Drosophila: insights from in vivo time lapse. *J. Neurosci.* **24**, 1541-1550.
Woods, A. J., White, D. P., Caswell, P. T. and Norman, J. C. (2004). PKD1/PKCmu promotes alphavbeta3 integrin recycling and delivery to nascent focal adhesions. *EMBO J.* **23**, 2531-2543.
Wu, G. Y. and Cline, H. T. (2003). Time-lapse in vivo imaging of the morphological development of Xenopus optic tectal interneurons. *J. Comp. Neurol.* **459**, 392-406.
Yin, D. M., Huang, Y. H., Zhu, Y. B. and Wang, Y. (2008). Both the establishment and maintenance of neuronal polarity require the activity of protein kinase D in the Golgi apparatus. *J. Neurosci.* **28**, 8832-8843.